



Assessment of the sea-ice carbon pump: Insights from a three-dimensional ocean-sea-ice biogeochemical model (NEMO-LIM-PISCES)

Sébastien Moreau^{1,2*} • Martin Vancoppenolle³ • Laurent Bopp⁴ • Oliver Aumont⁵ • Gurvan Madec^{3,6} • Bruno Delille⁷ • Jean-Louis Tison⁸ • Pierre-Yves Barriat¹ • Hugues Goosse¹

¹Georges Lemaître Centre for Earth and Climate Research, Earth and Life Institute, Université Catholique de Louvain, Louvain-La-Neuve, Belgium

²Institute for Marine and Antarctic Studies, University of Tasmania, Hobart, Tasmania

³Sorbonne Universités, UPMC Paris 6, LOCEAN-IPSL, CNRS, France

⁴Institut Pierre Simon Laplace/Laboratoire des Sciences du Climat et de l'Environnement, Centre National de la Recherche Scientifique, Gif sur Yvette, France

⁵Institut de Recherche Pour le Développement, Laboratoire de Physique des Océans, Brest, France

⁶National Oceanographic Centre, Southampton, United Kingdom

⁷Unité d'Océanographie Chimique, MARE, Université de Liège, Liège, Belgium

⁸Laboratoire de Glaciologie, Faculté des Sciences, Université Libre de Bruxelles, Bruxelles, Belgium

*s.moreau@uclouvain.be

Abstract

The role of sea ice in the carbon cycle is minimally represented in current Earth System Models (ESMs). Among potentially important flaws, mentioned by several authors and generally overlooked during ESM design, is the link between sea-ice growth and melt and oceanic dissolved inorganic carbon (DIC) and total alkalinity (TA). Here we investigate whether this link is indeed an important feature of the marine carbon cycle misrepresented in ESMs. We use an ocean general circulation model (NEMO-LIM-PISCES) with sea-ice and marine carbon cycle components, forced by atmospheric reanalyses, adding a first-order representation of DIC and TA storage and release in/from sea ice. Our results suggest that DIC rejection during sea-ice growth releases several hundred Tg C yr⁻¹ to the surface ocean, of which < 2% is exported to depth, leading to a notable but weak redistribution of DIC towards deep polar basins. Active carbon processes (mainly CaCO₃ precipitation but also ice-atmosphere CO₂ fluxes and net community production) increasing the TA/DIC ratio in sea-ice modified ocean-atmosphere CO₂ fluxes by a few Tg C yr⁻¹ in the sea-ice zone, with specific hemispheric effects: DIC content of the Arctic basin decreased but DIC content of the Southern Ocean increased. For the global ocean, DIC content increased by 4 Tg C yr⁻¹ or 2 Pg C after 500 years of model run. The simulated numbers are generally small compared to the present-day global ocean annual CO₂ sink (2.6 ± 0.5 Pg C yr⁻¹). However, sea-ice carbon processes seem important at regional scales as they act significantly on DIC redistribution within and outside polar basins. The efficiency of carbon export to depth depends on the representation of surface-subsurface exchanges and their relationship with sea ice, and could differ substantially if a higher resolution or different ocean model were used.

Introduction

For the sake of simplicity, the current representation of the role of sea ice in the carbon cycle in Earth System Models (ESMs) is minimalist (Orr et al., 2001). The sea ice is assumed to be biologically and chemically inactive; ocean-atmosphere gas fluxes vanish in ice-covered areas, or, better, depend linearly on ice fraction;

Domain Editor-in-Chief

Jody W. Deming,
University of Washington

Associate Editor

Lisa A. Miller,
Fisheries and Oceans Canada

Knowledge Domain

Ocean Science

Article Type

Research Article

Part of an *Elementa* Special Feature

Biogeochemical Exchange
Processes at Sea-Ice Interfaces
(BEPSII)

Received: December 18, 2015

Accepted: July 9, 2016

Published: August 3, 2016

and, in some cases, sea-ice formation and melt do not affect surface ocean concentrations of dissolved inorganic carbon (DIC) and total alkalinity (TA). However, observations have long indicated the existence of active biological and chemical processes within the sea ice (e.g., Vancoppenolle et al., 2013), gas exchanges are known to occur through permeable sea ice (e.g., Delille et al., 2014) and sea-ice growth and melt have a large impact on surface ocean chemical properties (e.g., Legge et al., 2015). Hence, the role of sea ice in the marine carbon cycle might be reconsidered and the representation of these processes in ESMs could be revised, which is the focus of this paper.

Sea-ice processes relevant to the marine carbon cycle are the following (see the schematic in Figure 1). The H₂O crystalline lattice hardly tolerates impurities, with most of them rejected from the ice by brine convection (Notz and Worster, 2008), increasing the surface ocean salinity, DIC and TA in the regions of net ice growth. When surface waters sink to depth, the anomalously large surface water DIC and TA can be exported downwards, providing a pathway for carbon sequestration. The small remainder of DIC and TA that is not rejected is stored within sea ice, transported by ice drift, and finally released to the ocean, impacting surface water properties in the regions of net ice melt. Besides these physical contributions, there are also active carbon processes in the ice. DIC can be exchanged with the atmosphere in the form of ice-atmosphere CO₂ fluxes (e.g., Miller et al., 2011; Papakyriakou and Miller, 2011; Geilfus et al., 2012; Nomura et al., 2013; see Figure 1). CaCO₃ precipitates in sea ice in the form of ikaite crystals (e.g. Dieckmann et al., 2008, 2010; Rysgaard et al., 2012, 2013), storing excess TA. Net community production (net primary production minus community respiration) occurs within sea ice through microbial communities, also impacting DIC and TA.

Of high relevance to the marine carbon cycle is the DIC budget in sea ice. Moreau et al. (2015) analysed this budget in detail, using a one-dimensional physical-biogeochemical process sea-ice model constrained by observations. They found a dominant role of physical processes (ice growth, melt and brine drainage) in the DIC budget, whereas ice-air gas fluxes, CaCO₃ formation and net community production were second-order processes. Also relevant to the marine carbon cycle is the TA/DIC ratio in sea-ice melt water, because changes in surface ocean TA/DIC ratio effectively influence ocean-atmosphere carbon fluxes (e.g., Bopp and Le Quéré, 2009). Sea-ice melt water has TA/DIC ratios between 1 and 2 (Rysgaard et al., 2007, 2009; Fransson et al., 2011; Miller et al., 2011; Geilfus et al., 2013; Brown et al., 2015), whereas this ratio is generally < 1 in seawater. The higher TA/DIC ratio in sea ice mostly results from active carbon processes in sea ice. Ikaite formation stores excess TA in the ice (Rysgaard et al., 2009). Ice-air CO₂ fluxes decrease the sea-ice DIC concentration and have been shown to lead to high sea-ice TA/DIC ratios (Moreau et al., 2015). Ice algae, the primary producers in sea ice, consume CO₂, hence decreasing DIC (Arrigo et al., 2010), and consume nitrate which increases alkalinity (Zeebe and Wolf-Gladrow, 2001). Upon ice melt, the release of DIC and excess TA by sea ice modifies the surface seawater pCO₂ and, therefore, ocean-atmosphere CO₂ fluxes. Hence, the chemical properties of melting sea ice are viewed as potentially influential to ocean-atmosphere CO₂ fluxes during the summer melt season (Delille et al., 2007; Rysgaard et al., 2011).

Here, we use an ocean general circulation model with representations of sea ice and the marine carbon cycle, in order to understand the impact of sea-ice processes on the carbon cycle, and to infer how they should be represented in ESMs. Rather than an explicit representation of all processes, we include simplified representations of the impact of two series of sea-ice processes on TA and DIC. The first are purely physical, including the impact of sea-ice growth, melt and brine drainage on TA and DIC in seawater. The second series of processes are active carbon processes within the sea ice (mainly CaCO₃ but also ice-atmosphere CO₂ exchanges and net community production), accounted for implicitly by changing the TA/DIC ratio in sea ice.

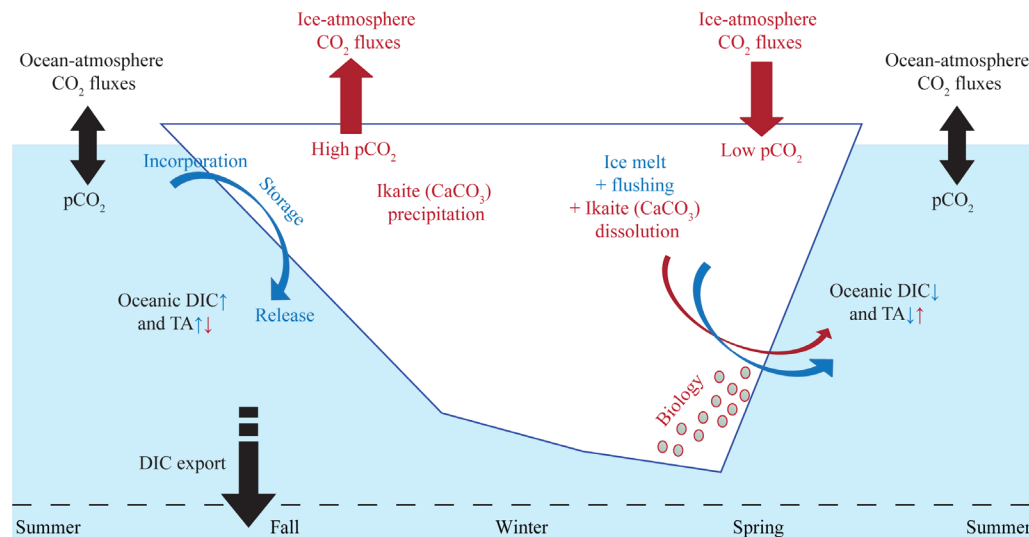


Figure 1
Schematic representation of the processes related to the role of sea ice in carbon cycling.

Schematic representation of the physical (blue) and active carbon (red) processes related to the role of sea ice in carbon cycling (for more details, see the Introduction). These processes include, from ice growth to ice melt (from left to right): the storage (incorporation minus brine drainage) of dissolved inorganic carbon (DIC) and total alkalinity (TA) by sea ice, the resulting change in surface water pCO₂ and ocean-atmosphere CO₂ fluxes, and the export of DIC to the deep ocean, the sea-ice active carbon processes of precipitation/dissolution of ikaite (CaCO₃), ice-atmosphere CO₂ fluxes, and impacts on DIC and TA by biological activities (green dots represent ice algae thriving in the bottom ice), the dilution of sea-surface DIC and TA by ice melt, the release of excess alkalinity (ikaite dissolution) by ice melt, and the resulting change in surface water pCO₂ and ocean-atmosphere CO₂ fluxes.

doi: 10.12952/journal.elementa.000122.f001

The model

We used the ocean modelling system NEMO 3.5 in its global ORCA2-LIM configuration, with the following specifications. The model has a quasi-isotropic tripolar grid with about 100 km in the Arctic and from about 100 to 50 km south of 60°S (Timmermann et al., 2005). There are 31 vertical z -levels, 20 of which located in the upper 500 m. The ocean component, OPA, is a primitive equation Boussinesq ocean model (Madec and the NEMO team, 2014). The sea-ice component is the Louvain-la-Neuve Ice Model (LIM2, Fichefet and Morales Maqueda, 1997; Timmermann et al., 2005). In the version that we used, the ice salinity, S_i , is prescribed at 6 g kg^{-1} everywhere except in the Baltic Sea, where it is 2 g kg^{-1} . The reference ice salinity of 6 g kg^{-1} is representative of the global mean (Vancoppenolle et al., 2009) and implicitly accounts for the effect of brine drainage. The marine biogeochemical component is the Pelagic Interaction Scheme for Carbon and Ecosystem Studies (PISCES, Aumont and Bopp, 2006; Aumont et al., 2015). Carbonate chemistry follows OCMIP-2 protocols and gas exchanges are parameterized according to Wanninkhof (1992), with the notable exception that the ocean-atmosphere gas flux is set to zero in the ice-covered part of the grid cells.

Surface ocean fluxes of DIC and TA

The ice-ocean tracer exchange formulation was modified from the original NEMO in order to allow for changes in sea-ice tracer concentrations, based on Roulet and Madec (2000). The ice-ocean tracer flux into the first ocean level due to sea-ice freezing, F , and melting, M , reads:

$$F_{\text{tracer}} = \frac{M - F}{\rho_0 \Delta z} C_i$$

where ρ_0 is the reference seawater density, Δz is the thickness of the first ocean level, and C_i is the tracer concentration (i.e., DIC and TA) in sea ice. Sea-ice freezing (melting) induces a net tracer concentration increase (decrease) in the uppermost ocean level. Our version of NEMO can use a rescaled z^* coordinate and embedded sea ice, following Campin et al. (2008).

Nevertheless, here we chose a z coordinate and a levitating sea ice, the options of an existing 3500 year-long spin-up simulation of the ocean carbon cycle used as initial state. With these choices, the model levels are fixed, the sea surface is linear, and there are no water exchanges between sea ice and the ocean. Therefore, a term, $-M - F\rho_0\Delta zC_0$, has to be added to F_{tracer} in order to mimic the effects of concentration/dilution associated with the ice-ocean water exchanges. Roulet and Madec (2000; see their Figure 5) show that this approach almost perfectly conserves the tracer content, as long as constant values for C_0 and C_i are used to compute the ice-ocean tracer fluxes.

Short 50-yr sensitivity experiments were run with respect to (i) the choice of constant versus interactive C_0 , (ii) the use of z^* versus z coordinates, and (iii) embedded versus levitating sea ice. None of these numerical choices affected our conclusions (not shown), which can be understood easily because the resulting perturbation is much smaller than the large seasonal signals investigated in this paper.

The choice of C_0 and C_i is the following: C_0 was derived from global annual mean values ($1988.6 \text{ mmol m}^{-3}$ of DIC and $2310.6 \text{ mmol m}^{-3}$ of TA; Table 1) at the end of the 3500-year spin-up simulation, while C_i was modified among the different sensitivity experiments. As for salt, an exception was enforced in the Baltic Sea, which is much fresher than the global ocean. There, seawater reference values for DIC and TA were derived from:

$$C_0^{\text{Baltic}} = C_0^{\text{global}} (S_0^{\text{Baltic}} / S_0^{\text{global}})$$

This approach does not take into account the fact that, for $S_0 = 0$, TA in the Baltic Sea is non-zero.

Table 1. Characteristics^a of the modelling experiments

Experiment ^b	Length (years)	Description	Ocean DIC (mmol m ⁻³)	Ice DIC (mmol m ⁻³)	Ocean TA (mmol m ⁻³)	Ice TA (mmol m ⁻³)
CTRL	500	control run	1988.6	1988.6	2310.6	2310.6
PHYS	500	sea ice DIC = 6/34 oceanic DIC	1988.6	343.9	2310.6	399.5
		sea ice TA = 6/34 oceanic TA				
CARB	500	sea ice DIC = 6/34 oceanic DIC	1988.6	343.9	2310.6	799
		sea ice TA = 12/34 oceanic TA				

^aThe oceanic concentrations used for dissolved inorganic carbon (DIC) and total alkalinity (TA) were global annual mean values at the end of the spin-up simulation (see text).

^bCTRL = a pre-industrial control, PHYS = sensitivity experiment with physical processes only, CARB = sensitivity experiment with active carbon processes.

doi: 10.12952/journal.elementa.000122.t001

Experiments

Three simulations were performed to investigate the sensitivity of the marine carbon cycle to solute fluxes of DIC and TA associated with sea-ice growth and melt (see Table 1 for a synthetic description). A pre-industrial setup was enforced by maintaining a constant atmospheric CO₂ concentration (278 µatm). All three experiments started from a 3500 year-long equilibrium spin-up, reaching quasi-equilibrium.

The atmospheric state was imposed using the CORE I normal year forcing set proposed by Large and Yeager (2009), developed to intercompare ice-ocean models (Griffies et al., 2009). It is based on a combination of NCEP/NCAR reanalyses (for wind, temperature and humidity) and various satellite products (for radiation), has a 2° resolution and near-zero global mean heat and freshwater fluxes. The so-called normal year data set superimposes the 1995 synoptic variability on the mean 1984–2000 seasonal cycle. Runoff biogeochemical properties were based on Ludwig et al. (1996). More details on the forcing data sets are available in Aumont et al. (2015).

In the control experiment (CTRL), the reference concentrations of tracers were assumed to take the exact same values in sea ice and in the surface seawater. In this case, the net solute flux due to sea-ice growth and melt vanishes, and the surface ocean concentration is only affected by evaporation minus precipitation.

In the first sensitivity experiment (so-called PHYS), DIC and TA are considered as passive tracers in sea ice, driven by the exact same processes as salt. Hence, the ice-ocean concentration ratio for DIC and TA follows salinity, and the reference concentrations of DIC and TA in sea ice are:

$$C_i = C_0 (S_i/S_0)$$

where $S_0 = 34.7 \text{ g kg}^{-1}$ (except in the Baltic Sea where $S_0 = 4 \text{ g kg}^{-1}$). This experiment has positive (negative) net solute flux to the surface ocean when ice grows (melts). The comparison PHYS-CTRL therefore isolates the role of concentration/dilution effects in seawater due to sea ice growth/melt (blue processes in Figure 1).

In the second sensitivity experiment (CARB), DIC in sea ice is still considered to behave as salt. TA, by contrast, is considered to be affected by active carbon processes in sea ice which may increase the ice-ocean ratio to twice that of salt and DIC, corresponding to a high limit of the TA/DIC ratio in sea ice (Rysgaard et al., 2013). In this experiment, a relatively larger amount of TA as compared to DIC is stored in sea ice (released to the surface ocean) during growth (melt). Hence, under-ice waters are left depleted (enriched) in TA as compared to DIC in regions of sea ice growth (melt). The comparison CARB-PHYS isolates the role of the biogeochemical sea ice processes (ikaite precipitation, air-ice CO₂ fluxes and net community production) which, in some conditions, would lead to a sea-ice TA/DIC ratio of about 2 (cf. the Introduction and red processes in Figure 1). This particular set-up, however, reflects the role of ikaite precipitation which stores excess alkalinity in sea ice, rather than the roles of ice-atmosphere CO₂ fluxes and primary production which mostly decrease DIC in sea ice. The seasonality of these latter processes is not considered in these simulations; the assumption of time-independent DIC and TA values in sea ice implicitly rules out direct ice-atmosphere CO₂ exchange and primary production. All three simulations (CTRL, PHYS, and CARB) were run for 500 years after the 3500 year-long spin-up.

Results

In this section, the Arctic Ocean refers to waters north of 66°N and the Southern Ocean to waters south of 50°S. The forthcoming analysis focuses on the last of the 500 years of model run and on the sea-ice impacts on the regional and global marine carbon cycle.

Sea-ice growth and melt, and marine carbon cycle in the CTRL simulation

In the Arctic Ocean, this control (preindustrial) simulation indicates that sea ice grows the most along coastal shelves and less so in the central Arctic (Figure 2a). From there, sea ice drifts following the cyclonic Beaufort Gyre and the transpolar drift and melts mostly in the marginal ice zones, in particular in the Labrador and West Greenland Seas (sometimes south of the Arctic circle), and also in the Beaufort and Chukchi Seas (Figure 2b). In the Southern Ocean, sea ice grows mainly in coastal polynyas along the Antarctic continent, and moderately within the pack ice zone (Figure 2d). Sea ice then melts, mainly within the pack ice zone, and retreats southward (Figure 2e).

The Arctic DIC and TA distributions in surface waters (Figure 3a and b) roughly follow salinity, being highest in the North Atlantic and the Hudson Bay, intermediate in Pacific waters, and lowest on the Siberian Shelf, under the influence of freshwater from rivers. At the regional scale, large uncertainties remain in the DIC and TA values, which have not been compared to observations, particularly for shallow coastal regions. For example, the Hudson Bay has fairly high DIC (close to 2200 mmol m⁻³) in the CTRL while observations show lower concentrations (about 2000 mmol m⁻³; Azetsu-Scott et al., 2014). The Arctic surface waters are generally undersaturated in CO₂ (Figure 3c). For this reason, the pre-industrial Arctic Ocean simulated here is a sink for atmospheric CO₂ (with negative CO₂ fluxes, i.e., from atmosphere to ocean; Figure 3d).

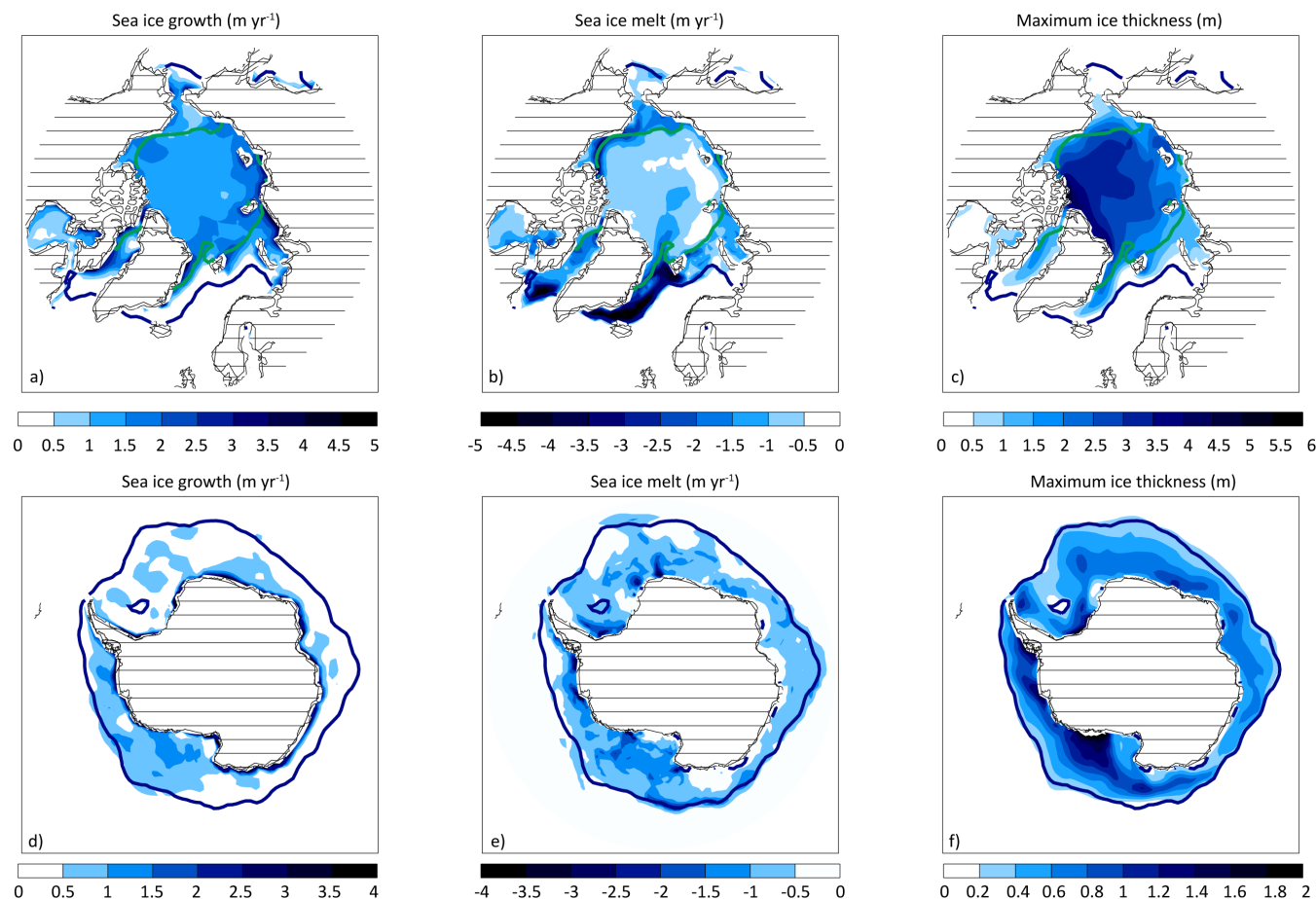


Figure 2
 Simulated sea ice growth, melt and maximum thickness.

Modelled net ice growth (m yr^{-1}), net ice melt (m yr^{-1}) and maximum ice thickness (m) in the Arctic Ocean (upper panels a–c) and the Southern Ocean (lower panels d–f). The green and blue lines indicate the minimum and maximum sea ice extent, respectively. The textured areas indicate the model grid.

doi: 10.12952/journal.elementa.000122.f002

A notable exception is the Siberian Shelf, where the applied river runoff is rich in DIC and depleted in TA, which drastically increases $p\text{CO}_2$ above the atmospheric value. Hence, coastal Kara and Laptev Seas are source regions for atmospheric CO_2 . The CO_2 flux sign depends on the atmosphere–ocean $p\text{CO}_2$ difference, whereas its magnitude is clearly influenced by sea-ice concentration, with much smaller values in the sea-ice zone than elsewhere.

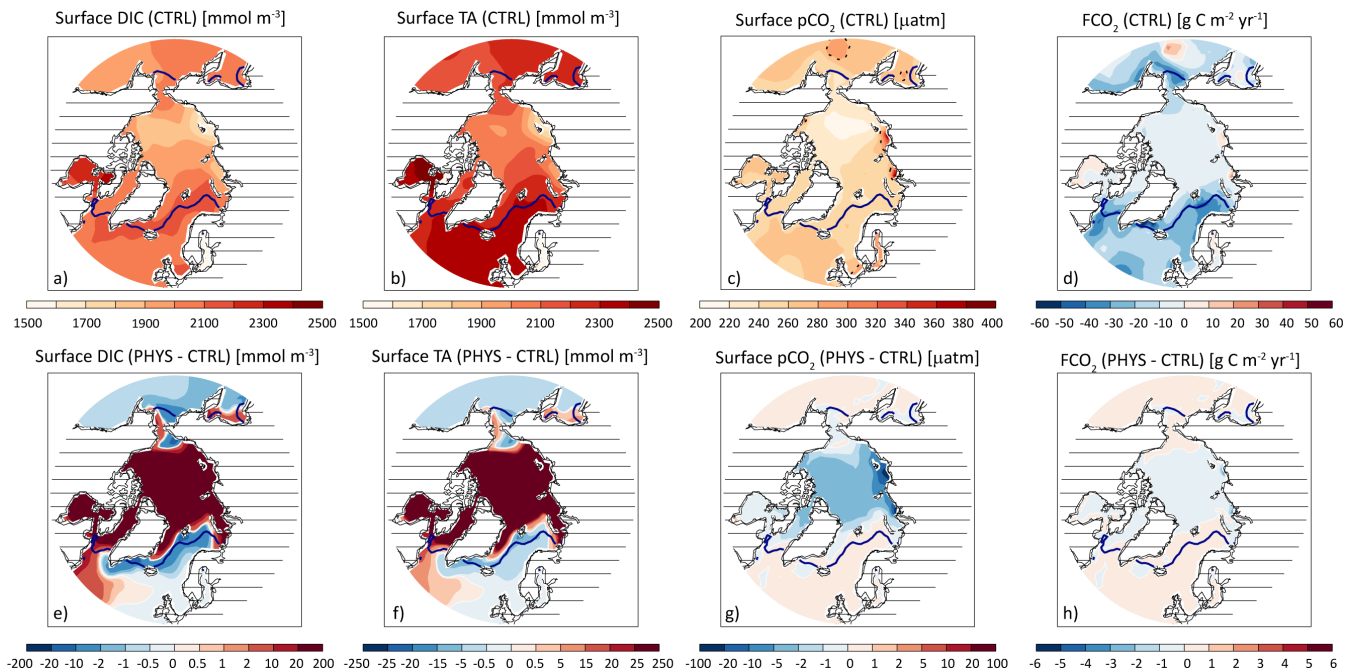
Antarctic surface concentrations in DIC and TA (Figure 4a and b) are highest along the Antarctic coast, peak in the Weddell Gyre, and decrease northwards. The surface $p\text{CO}_2$ roughly follows the same pattern and is generally higher than the atmospheric value. Therefore, in this simulated pre-industrial situation, the Antarctic region is a source for atmospheric CO_2 (with positive CO_2 fluxes, i.e., from ocean to atmosphere, Figure 4d). The impact of ice concentration on the CO_2 flux is, as in the Arctic, clearly visible (Figure 2c and f).

PHYS-CTRL: Effect of DIC rejection during growth, and freshwater dilution during melting

Arctic Ocean

The PHYS-CTRL differences in sea-surface DIC and TA are dominated by patterns of ice growth and melt. Sea ice stores less DIC and TA in PHYS than in CTRL, hence, there are large positive anomalies of DIC and TA where ice forms, and in particular in the Siberian Shelf polynyas where large amounts of ice form and are exported every year (see net annual increase in Figure 3e and f). There are also notable negative anomalies in regions of net annual melting (North Atlantic, Chukchi Sea). Where intense, the ocean circulation tends to dilute the signal, in particular in the North Atlantic. Since the TA/DIC ratio does not change much, and because only changes in surface ocean TA/DIC ratio can significantly change ocean–atmosphere carbon fluxes (e.g., Bopp and Le Quéré, 2009), the resulting $p\text{CO}_2$ changes are generally small (Figure 3g). The only exceptions are the negative $p\text{CO}_2$ anomalies in the coastal Kara and Laptev Seas which result from the combination of DIC-rich and TA-depleted river runoff with sea-ice growth.

Overall, the net PHYS effect is to make the Arctic a slightly more efficient sink for atmospheric ocean CO_2 (with more negative CO_2 fluxes; Figure 3h), mostly driven by the weaker CO_2 source in the Kara and Laptev Seas. Integrated over the entire Arctic Ocean, this effect corresponds to a small extra uptake



of atmospheric carbon ($< 1 \text{ Tg C yr}^{-1}$; Figure 5a), which, over the 500 years of the run, would add about $1 \text{ Tg C yr}^{-1} \times 500 \text{ yr} = 0.5 \text{ Pg C}$ in the Arctic Ocean in PHYS, as compared to CTRL.

This amount of 0.5 Pg C is not enough to explain the total simulated extra DIC in Arctic waters (2.3 Pg C after 500 years; Figure 5c and 6). The extra 1.8 Pg C in the deep Arctic Ocean correspond to the amount of carbon rejected from forming ice and stored at depth in net growth regions (in PHYS), whereas this carbon stays in the ice upon formation and is transported to regions of net ice melt in CTRL. Indeed, every winter, there is about $13,400 \text{ km}^3$ of ice growth which in the CTRL has no impact on DIC, whereas this releases about 270 Tg C yr^{-1} in the surface ocean for PHYS. An approximate 1.4% export fraction of this extra surface DIC to depth by vertical ocean mixing is enough to explain the extra 1.8 Pg C accumulated within the Arctic basin over 500 years.

This extra storage of carbon is compensated by the following mechanism. Every summer, a large part of sea-ice volume is exported and melts in Labrador and West Greenland Seas. The waters south of Greenland, where deep convection occurs in the model, are thus depleted in DIC (Figure 6). Therefore, the waters exported to depth by deep convection are depleted in carbon by comparison to CTRL, which is visible in the entire North Atlantic basin. Overall, this reduced carbon transport by drifting ice in PHYS as compared to CTRL induces a redistribution of carbon, from sub-Arctic regions to the central Arctic.

Southern Ocean

In the Southern Ocean, there are significant increases in PHYS surface DIC and TA in coastal regions where sea ice grows, and significant decreases away from the continent where it melts (Figure 4e and f). The changes in surface $p\text{CO}_2$ are small, being slightly negative near the coasts and slightly positive offshore. These small changes induce slightly higher CO_2 fluxes in PHYS than in CTRL (Figure 4h).

Integrated over the whole Southern Ocean in PHYS, the higher CO_2 fluxes lead to an extra approximate $1 \text{ Tg C yr}^{-1} \times 500 \text{ yr} \approx 0.5 \text{ Pg C}$ (after 500 yr) to the atmosphere (Figure 5a); i.e., the Southern Ocean is a larger source of atmospheric CO_2 in PHYS than in CTRL. However, the Southern Ocean is gaining about 1.5 Pg C in 500 yr in PHYS as compared to CTRL (Figure 5c), hence vertical carbon export must explain an anomalous 2 Pg C , which requires that about 2% of the 204 Tg C released by coastal sea-ice formation every winter is exported to depth. In contrast to the Arctic Ocean, this excess DIC is entrained northward along newly formed deep waters (Figure 6).

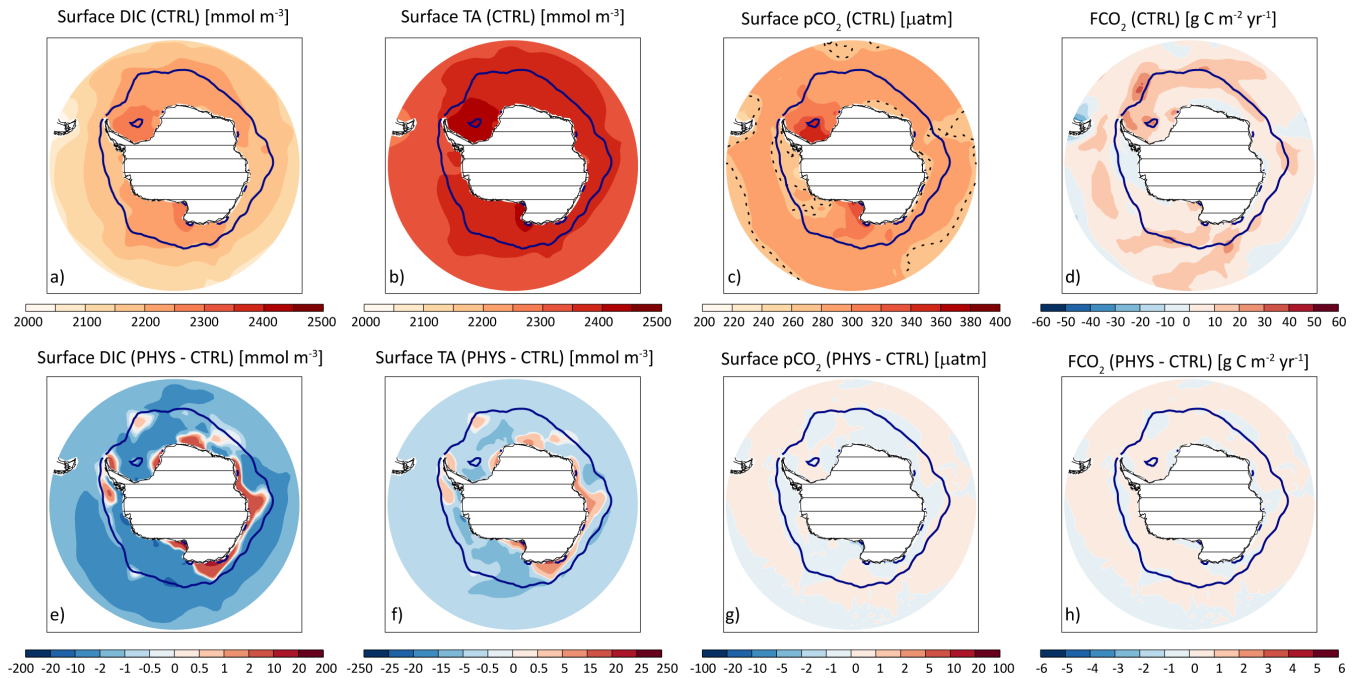
This increase at depth due to winter processes is compensated by the effect of freshwater export, poor in DIC, by melting sea ice away from the continent, spreading to the entire mid-latitude and tropical ocean surface and causing a slight decrease in CO_2 fluxes (Figure 6). Overall, this reduced carbon transport by drifting ice in PHYS as compared to CTRL induces a redistribution of carbon, with larger values in high latitudes and reductions at lower latitudes, without net significant change in the total amount of carbon (Figure 5c).

Figure 3

CTRL results and PHYS-CTRL differences in Arctic Ocean surface DIC, TA, $p\text{CO}_2$ and CO_2 fluxes.

Model results for the CTRL experiment (upper panels a–d) and for differences between the PHYS sensitivity and CTRL experiments (PHYS-CTRL, lower panels e–f), after 500 years of run, for the mean annual sea-surface DIC (mmol m^{-3}), TA (mmol m^{-3}), $p\text{CO}_2$ (μatm), the dashed line shows the $278 \mu\text{atm}$ contour, and CO_2 fluxes ($\text{FCO}_2, \text{g C m}^{-2} \text{ yr}^{-1}$) in the Arctic Ocean (see Table 1 for characteristics of the experiments). FCO_2 is expressed in $\text{g C m}^{-2} \text{ yr}^{-1}$ for ease of comparison to other values provided elsewhere. The blue line indicates the maximum winter sea ice extent; the textured areas indicate the model grid. For ease of comparison between figures, the color scales used for the PHYS-CTRL differences depicted here are the same as for the PHYS-CTRL differences depicted in Figure 4 for the Southern Ocean.

doi: 10.12952/journal.elementa.000122.f003



CARB-PHYS: The role of high TA/DIC ratios

Arctic Ocean

In CARB, twice as much TA is stored in sea ice as compared to PHYS. Hence, surface TA decreases in regions of net annual growth (the Central Arctic and the Siberian Shelf), and increases in regions of net annual melt, most notably in the Greenland and Labrador Seas (Figure 7b). Compared to PHYS, the surface ocean TA/DIC ratio significantly changes in CARB (by as much as -0.02 in regions of net ice growth). Hence, significant $p\text{CO}_2$ differences are found, and these are, as expected, opposite to TA differences. In CARB, the surface $p\text{CO}_2$ is higher than in PHYS in the Central Arctic and along the Siberian Shelf, and lower in the Greenland and Labrador Seas (Figure 7c). However, because of the high winter ice concentrations in the Central Arctic, this $p\text{CO}_2$ difference does not translate into an annual mean CO_2 flux difference. The latter is instead dominated by summer $p\text{CO}_2$ differences (Figure 7h and i). On an annual basis, a weaker (stronger) CO_2 sink is found in CARB where ice grows (melts) (Figure 7d). Because the treatment of DIC is exactly the same in PHYS and CARB, changes in DIC must come from impacts of TA changes on $p\text{CO}_2$ and CO_2 fluxes. As a result, the surface DIC is slightly lower in CARB than in PHYS where ice forms, and higher where ice melts (see Figure 7a).

In about 30 years, the net Arctic-integrated ocean-atmosphere sink for atmospheric CO_2 becomes about 4 Tg C yr^{-1} weaker in CARB than in PHYS (Figure 5b). After 500 years, the Arctic Ocean in CARB has released (or more exactly not absorbed) an extra $4 \text{ Tg C yr}^{-1} \times 500 \text{ yr} = 2 \text{ Pg C}$ as compared to PHYS. However, the total DIC is only about -0.1 Pg C lower in CARB than in PHYS (Figure 5d). The missing -1.9 Pg C are due to i) export of a negative DIC anomaly to the North Atlantic through Baffin Bay and Davis Strait (Figure 7a and 9) and ii) positive DIC anomalies in the Barents and East Siberian Seas (Figure 7a). Therefore, while the PHYS-CTRL differences are mostly due to the changes in DIC transport by sea ice, with DIC anomalies confined to the Arctic basin, the CARB-PHYS differences are mostly explained by changes in surface ocean CO_2 flux anomalies and involve changes outside the Arctic basin. Finally, the much smaller size of the DIC changes in CARB-PHYS as compared to PHYS-CTRL (Figures 6 and 9) is because the TA-driven CO_2 flux anomaly in CARB-PHYS is much smaller than the extra 270 Tg C yr^{-1} released in the winter surface ocean in PHYS as compared to CTRL.

Southern Ocean

Comparable mechanisms are found in the Southern Ocean but give a contrasting DIC response. Where ice grows (near coastal polynyas), the surface ocean TA is lower in CARB than in PHYS (Figure 8b), and where ice melts offshore in the Southern Ocean, surface TA is higher. The annual surface $p\text{CO}_2$ anomaly does not exactly match the annual TA anomaly (e.g., off the Ross Sea, Figure 8c), due to the presence of sea ice during the ice-growing season (May to September). At this time of the year, surface TA mostly decreases around Antarctica in CARB compared to PHYS (Figure 8f), which increases the surface ocean $p\text{CO}_2$ (Figure 8g). However, because of the presence of sea ice, this increase has no effect on ocean-atmosphere CO_2 fluxes (Figure 8h). During winter, in contrast to the Arctic, this negative TA anomaly is exported to depth because

Figure 4

CTRL results and PHYS-CTRL differences in Southern Ocean surface DIC, TA, $p\text{CO}_2$ and CO_2 fluxes.

Model results for the CTRL experiment (upper panels a-d) and differences between the PHYS sensitivity and CTRL experiments (PHYS-CTRL, lower panels e-f), after 500 years of run, for the mean annual sea-surface DIC (mmol m⁻³), TA (mmol m⁻³), $p\text{CO}_2$ (μatm, the dashed line shows the 278 μatm contour), and CO_2 fluxes (FCO₂, g C m⁻² yr⁻¹) in the Southern Ocean (see Table 1 for characteristics of the experiments). FCO₂ is expressed in g C m⁻² yr⁻¹ for ease of comparison to other values provided elsewhere. The blue line indicates the maximum winter sea ice extent; the textured areas indicate the model grid. For ease of comparison between figures, the color scales used for the PHYS-CTRL differences depicted here are the same as for the PHYS-CTRL differences depicted in Figure 3 for the Arctic Ocean.

doi: 10.12952/journal.elementa.000122.f004

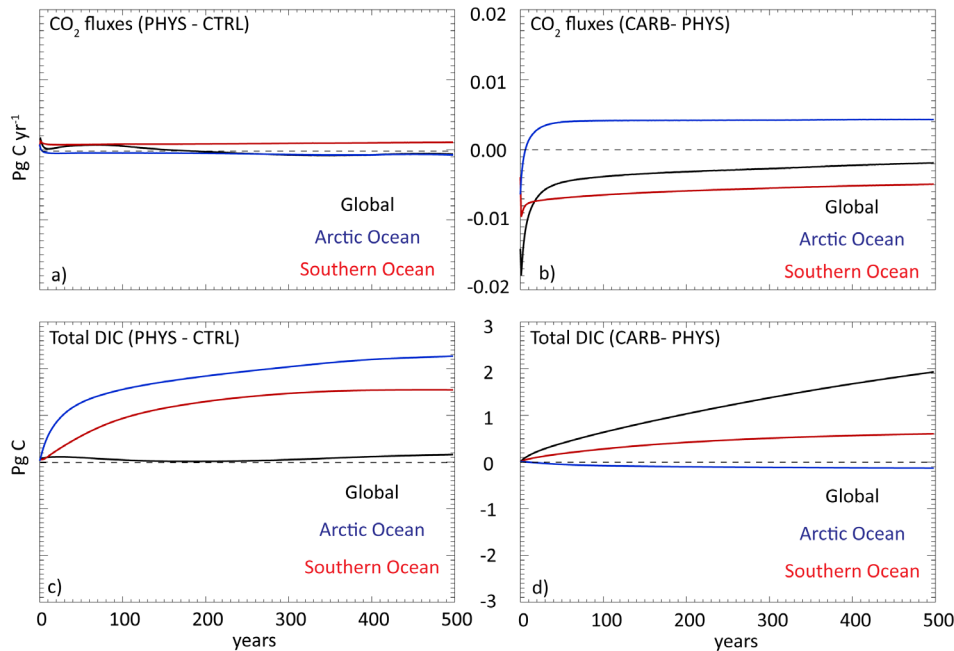


Figure 5
Differences in CO₂ fluxes and total DIC between experiments for the Arctic and Southern Oceans.

Modelled differences in CO₂ fluxes (Pg C yr⁻¹) between a) the PHYS sensitivity and CTRL experiments (PHYS-CTRL) and b) the CARB and PHYS sensitivity experiments (CARB-PHYS; see Table 1 for characteristics of the experiments), and in the total DIC (Pg C) for c) PHYS-CTRL and d) CARB-PHYS, for 500 years of run, for the Arctic Ocean (blue), the Southern Ocean (red) and the Global Ocean (black).

doi: 10.12952/journal.elementa.000122.f005

of stronger vertical mixing. Hence, when the vast expanses of TA-enriched sea ice melt in spring, TA sharply increases in CARB as compared to PHYS (Figure 8j). This increase is the key difference from the Arctic. In the Southern Ocean, it decreases the surface *p*CO₂ in the summer (Figure 8k). Because the ice concentration is small in summer, this decrease can reduce the CO₂ fluxes to the atmosphere (Figure 8l). In turn, on an annual basis, in CARB there is a net reduction in CO₂ fluxes around most of the Southern Ocean (Figure 5b and 8d), so that DIC increases in both regions of deep water formation and regions of ice melt (Figure 8a).

After 500 years, the Southern Ocean is a net lower CO₂ source in CARB (about -5 Tg C yr⁻¹, Figure 5b). This effect drives an accumulation of DIC in the Southern Ocean of about 5 Tg C yr⁻¹ × 500 years ≈ 2.5 Pg C. Because the accumulation of DIC takes place both offshore and in deep water formation zones, DIC increases in both surface and deep waters of the Southern Ocean and extends northwards (Figure 8a and 9). After 500 years, the total DIC content of the Southern Ocean has only increased by about 0.6 Pg C (Figure 5d) in CARB compared to PHYS. A large part of the excess DIC has been transported north of the Southern Ocean (Figure 9) and contributed in part to the global increase in DIC (about 1.9 Pg C after 500 years; Figure 5d). The residual 0.6 Pg C has been released back to the atmosphere in mid-latitude and tropical regions (Figure 9). Hence, contrary to PHYS, CARB has a small effect on the total DIC of the Southern Ocean but a more important effect on the global storage of DIC.

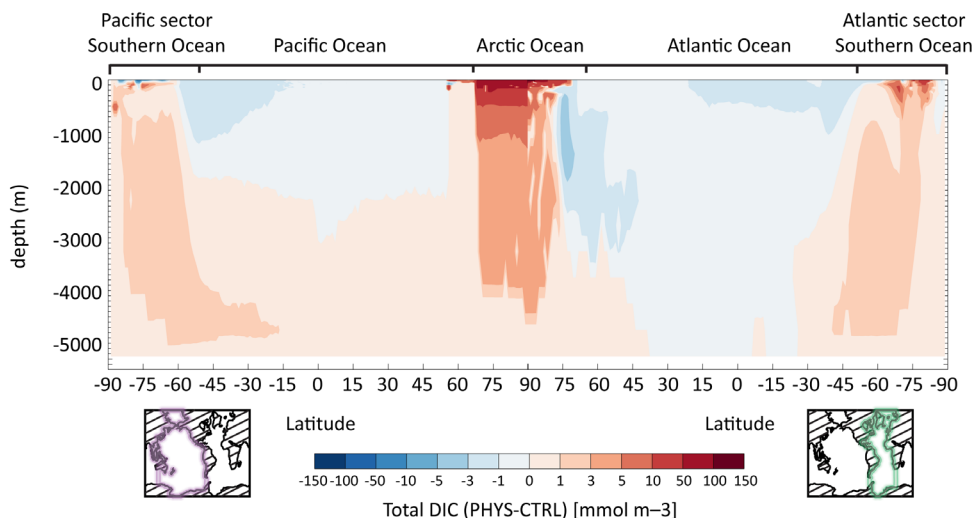
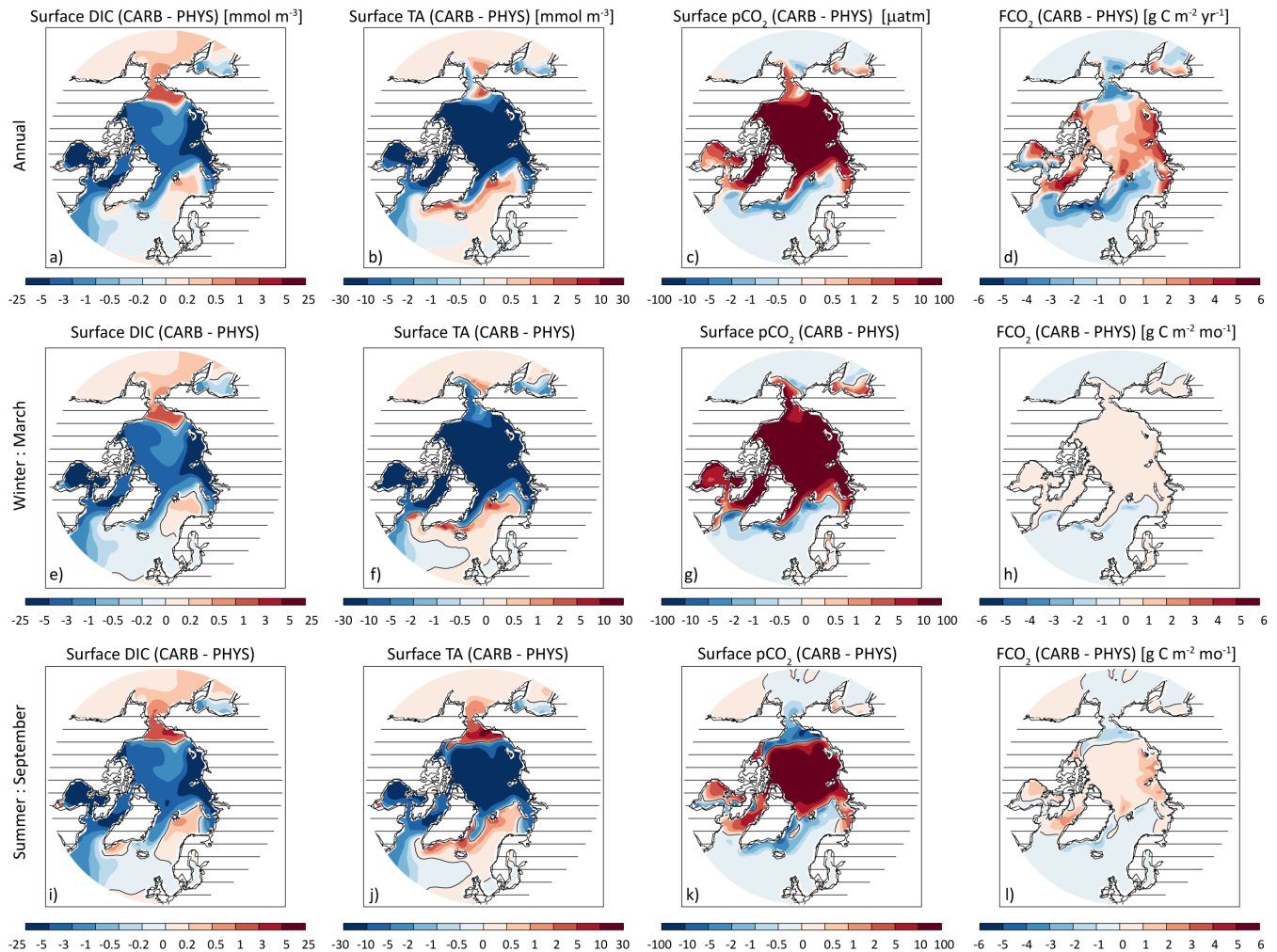


Figure 6
Total DIC differences between PHYS and CTRL experiments for the global ocean.

Sector mean (through the Pacific and the Atlantic Oceans) of the total DIC difference (mmol m⁻³) between the PHYS and CTRL experiments.

doi: 10.12952/journal.elementa.000122.f006



Discussion

What is the role of physical and active carbon sea-ice processes in the pre-industrial marine carbon cycle?

The physical processes (sea-ice growth and melt and carbon-rich brine rejection) activated in the PHYS simulation trigger a chain of processes moving a few Pg of carbon to the polar deep ocean basins in 500 years of simulation. This physical sea-ice carbon pump relies on (i) the annual mobilization of hundreds of Tg C in the under-ice ocean surface by brine rejection during sea-ice growth, (ii) the export of a small fraction (< 2%) of this carbon to the deep ocean by vertical exchange processes and currents, and (iii) the large dilution of surface DIC by melting sea ice in summer. In the Southern Ocean, this dilution constitutes a negative northward carbon flux that compensates for the transport of carbon to the mid-latitude deep ocean. In the Arctic Ocean, the transport of carbon to the deep ocean stays confined within the Arctic Basin. Overall, PHYS redistributes DIC to high latitudes (Figure 10b and e). Because it does not directly modify the TA/DIC ratio in surface waters, the physical sea-ice carbon pump leaves the ocean-atmosphere carbon fluxes hardly changed.

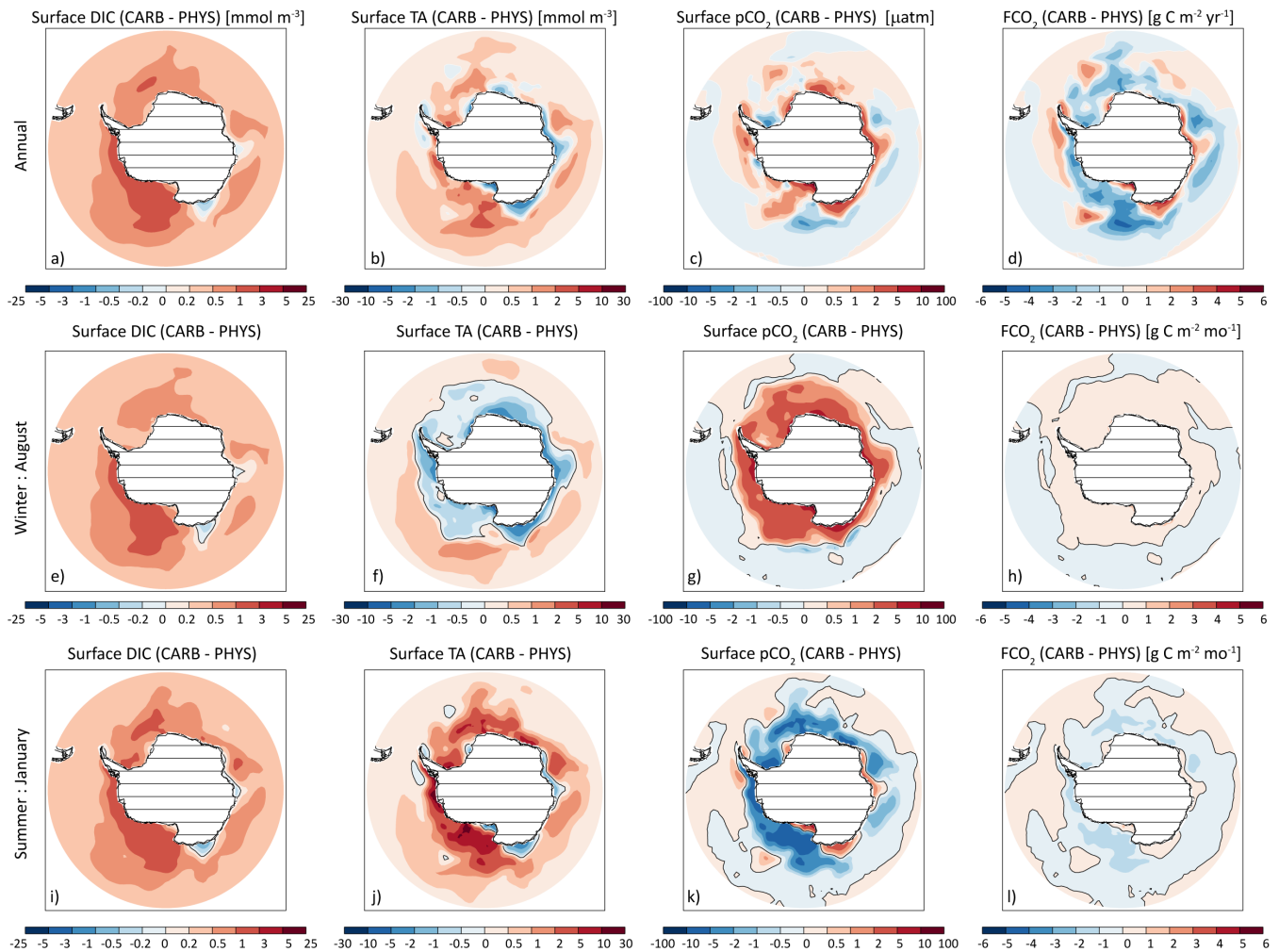
Active carbon processes that affect TA/DIC in sea ice, implicitly accounted for in the CARB simulation, activate a biogeochemical sea-ice carbon pump. Because they affect the TA/DIC ratio, such processes are able to affect the net ocean-atmosphere CO_2 exchange by a few Tg C per year in the sea-ice zone, with opposite signs in the two hemispheres. The DIC content of the Arctic Ocean decreases slightly and a negative DIC anomaly is exported to the North Atlantic through Baffin Bay and Davis Strait (Figure 9 and 10c). In the Southern Ocean, DIC increases in both surface and deep waters and this accumulation extends northwards (Figure 9 and 10f). The key difference is the ability of the Southern Ocean to export winter negative alkalinity anomalies, whereas in the Arctic such anomalies remained confined to the surface. Overall, CARB leads to the introduction of an extra 2 Pg C in the global ocean in 500 years, mostly due to a less efficient Southern Ocean source of atmospheric CO_2 . This extra carbon stock in the deep ocean would build up further if the

Figure 7

CARB-PHYS differences in surface DIC, TA, pCO_2 and CO_2 fluxes in the Arctic Ocean.

Annual (upper panels a–d), winter (middle panels e–h) and summer (lower panels i–l) differences between the CARB and PHYS sensitivity experiments (CARB-PHYS), after 500 years of run, in the sea-surface DIC (mmol m^{-3}), TA (mmol m^{-3}), pCO_2 (μatm) and CO_2 fluxes (FCO_2 , $\text{g C m}^{-2} \text{yr}^{-1}$) in the Arctic Ocean (see Table 1 for characteristics of the experiments). FCO_2 is expressed in $\text{g C m}^{-2} \text{yr}^{-1}$ for ease of comparison to other values provided elsewhere. The textured areas indicate the model grid. For ease of comparison between figures, the color scales used for the CARB-PHYS differences depicted here are the same as for the CARB-PHYS differences depicted in Figure 8 for the Southern Ocean.

doi: 10.12952/journal.elementa.000122.f007



simulations were continued, as the CARB simulation is clearly not in equilibrium after 500 years (Figure 5d). The induced changes in ocean carbon storage are distributed globally and not confined to the polar deep basins.

With the present results, it is difficult to argue how sea ice could affect the global marine carbon cycle in contemporary ocean models. Indeed, the approximate 4 Tg C yr⁻¹ absorbed by the global ocean due to CARB processes (2 Pg C after 500 years) is rather low. Any changes in such a process over the last decades – or the coming ones – would probably not influence the global ocean annual CO₂ sink, estimated at 2.6 ± 0.5 Pg C yr⁻¹ (Le Quéré et al., 2015). However, sea-ice carbon processes act at the millennial scales of the ocean circulation and could reveal more importance at longer time scales. At least sea-ice carbon processes seem important at regional scales. Indeed, the hundreds of Tg C mobilized every year in the surface ocean under sea ice by brine rejection are much larger than recent estimations of the CO₂ sink in the Southern Ocean (50 Tg C year⁻¹, Takahashi et al., 2009). The changes in ocean-atmosphere CO₂ fluxes induced by active sea-ice biogeochemistry (+4 and -4 Tg C yr⁻¹ in the Arctic and Southern Oceans, respectively) also scale with these figures. Moreover, sea-ice processes significantly act on the redistribution of DIC and TA within and outside polar basins.

Is a strong sea-ice carbon pump suggested by Rysgaard et al. (2007, 2011) supported by our simulations?

Qualitatively, the answer is yes, as the suggested mechanisms driving the physical and biogeochemical carbon pumps are simulated by the model: we indeed see synergies between air-ice CO₂ fluxes, sea-ice growth and melt, TA/DIC ratios in sea ice, and deep ocean ventilation. The effects of these mechanisms, however, cannot be qualified as strong. A direct comparison with the results of Rysgaard et al. (2011) is difficult, because the box model they used was applied over a single seasonal cycle of sea-ice growth and melt for the

Figure 8

CARB-PHYS differences in surface DIC, TA, pCO₂ and CO₂ fluxes in the Southern Ocean.

Annual (upper panels a–d), winter (middle panels e–h) and summer (lower panels i–l) differences between the CARB and PHYS sensitivity experiments (CARB-PHYS), after 500 years of run, in the sea-surface DIC (mmol m⁻³), TA (mmol m⁻³), pCO₂ (µatm) and CO₂ fluxes (FCO₂, g C m⁻² yr⁻¹) in the Southern Ocean (see Table 1 for characteristics of the experiments). FCO₂ is expressed in g C m⁻² yr⁻¹ for ease of comparison to other values provided elsewhere. The textured areas indicate the model grid. For ease of comparison between figures, the color scales used for the CARB-PHYS differences depicted here are the same as for the CARB-PHYS differences depicted in Figure 7 for the Arctic Ocean.

doi: 10.12952/journal.elementa.000122.f008

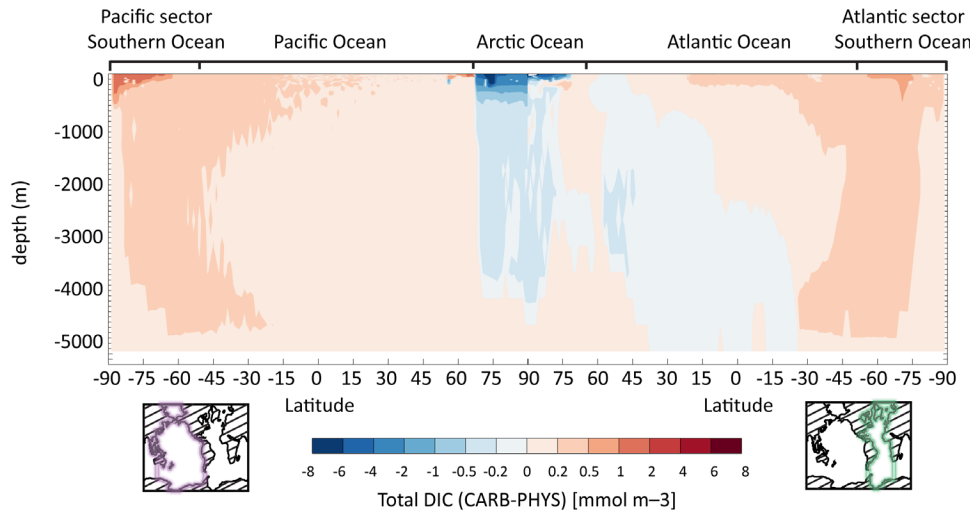


Figure 9
Total DIC differences between CARB and PHYS experiments for the global ocean.

Sector mean (through the Pacific and the Atlantic Oceans) of the total DIC differences (mmol m^{-3}) between the CARB and PHYS experiments.

doi: 10.12952/journal.elementa.000122.f009

contemporary carbon cycle, whereas we have used a global ocean GCM under pre-industrial conditions run over 500 years. In terms of the mobilization of carbon in surface waters due to the rejection of DIC-rich brine by growing sea ice, the Rysgaard et al. (2011) estimates of $138/186 \text{ Tg C yr}^{-1}$ in the surface Arctic/Southern Oceans are of the same order of magnitude as our computations ($266/204 \text{ Tg C yr}^{-1}$). The differences are due to the annual sea-ice formation, which is slightly larger in NEMO-LIM ($13.4/10.3 \times 10^3 \text{ km}^3 \text{ yr}^{-1}$) than what Rysgaard et al. (2011) assumed ($8.5/9.9 \times 10^3 \text{ km}^3 \text{ yr}^{-1}$) for the Arctic and Southern Oceans, respectively.

Where our respective studies disagree is in the amount of carbon exported below the mixed layer. Rysgaard et al. (2011) hypothesize that all DIC-rich brine would leave the mixed layer to the deep ocean, which magnifies carbon export at depth, whereas NEMO-LIM suggests that only 1.4% of the surface DIC rejected from growing sea ice is exported to the deep Arctic Ocean, and only about 2% to the deep Southern Ocean. That these fractions are small does not seem surprising as (i) sea ice does not grow only where deep water forms, (ii) deep water properties are diluted on their way downwards, and (iii) there are exchanges between the deep ocean and the surface that resupply some of the deep carbon to the surface.

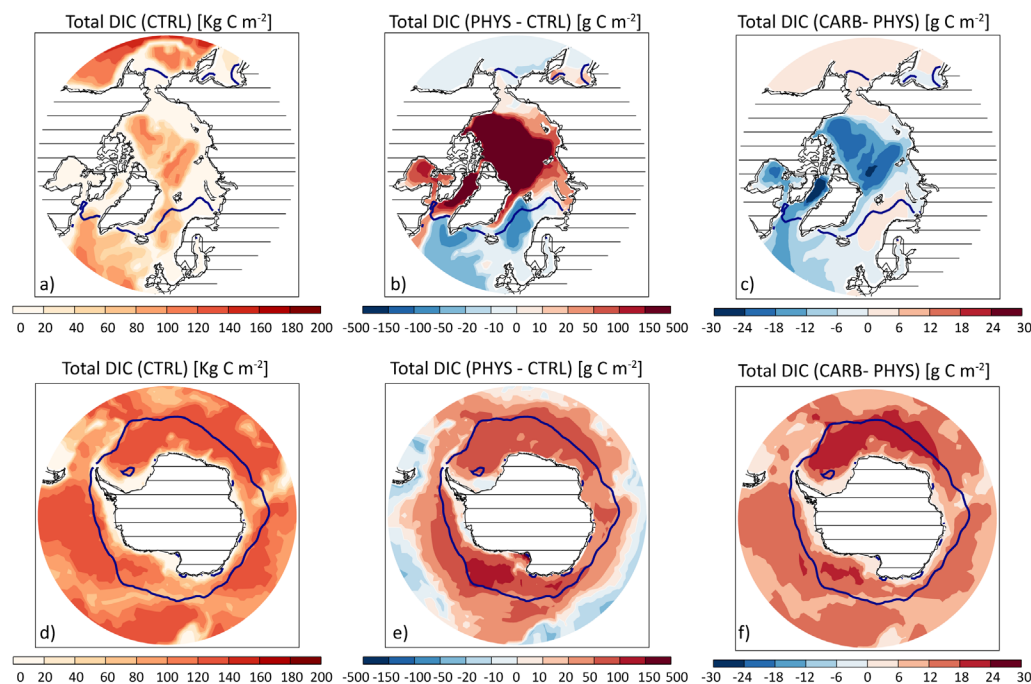


Figure 10
CTRL total DIC and differences in PHYS-CTRL and CARB-PHYS in the Arctic and Southern Oceans.

Total DIC (kg C m^{-2}) in the CTRL experiment and differences in total DIC (g C m^{-2}) in the PHYS-CTRL and CARB-PHYS comparisons, after 500 years of run, for the Arctic Ocean (a-c) and the Southern Ocean (d-f).

doi: 10.12952/journal.elementa.000122.f010

How robust are our conclusions?

The conclusions presented here are based on a single ocean modelling system, which is by essence subject to errors. First, the strength of the physical and biogeochemical carbon pump depends on sea-ice dynamics, ocean circulation, and the ability of vertical processes to export carbon to depth. The amount of sea ice

formed every year is in line with other model estimates (e.g., Chevallier and Salas-Mélia, 2012) and would not hugely change if another sea-ice model was used. The distribution of sea ice is also reasonable, as shown by previous studies (Timmermann et al., 2005). Where differences could arise is in the representation of ocean currents and vertical exchanges if resolution was increased to eddy-permitting or eddy-resolving simulations. The strength of the biogeochemical carbon pump depends solely on the TA/DIC ratio in sea ice, which was chosen at the extreme limit of observations here (Rysgaard et al., 2013), hence it would likely be smaller in general. Similar experiments to ours were performed using a different model (MPIOM-HAMOCC; Grimm et al., pers. comm.). The results of these latter simulations are in line with ours, which strengthens the confidence in our findings.

There are also missing processes that seemed of less importance a priori, but which scale with the simulated changes; i.e., air-ice CO₂ fluxes (~ 30 Tg C yr⁻¹; Delille et al., 2014) and primary production in sea ice (~ 10 Tg C yr⁻¹; Deal et al., 2011; Saenz and Arrigo, 2014). These processes would be needed to be considered in more detailed studies. Hence, this study is only a first step towards understanding the global implications of carbon processes in the sea-ice zone. The findings from this first step suggest that sea-ice processes need to be considered in present-day marine carbon cycle studies if the scales of interest are regional, but likely not if the latter are global. Finally, sea-ice processes could have stronger effects on the marine carbon cycle in climates where the seasonal cycle is much stronger (e.g. the Last Glacial Maximum, Clark et al., 2009) or if integrated over longer time scales (i.e., until equilibrium is reached).

Key findings

Our modelling results suggest that only 1.4% of the surface DIC rejected from growing sea ice is exported to the deep Arctic Ocean, and only about 2% to the deep Southern Ocean. These fractions seem small, but they are not surprising as (i) sea ice does not grow only where deep water forms, (ii) deep water properties are diluted on their way downwards, and (iii) there are exchanges between the deep ocean and the surface that resupply some of the deep carbon to the surface. On the contrary, the strength of the physical and biogeochemical carbon pump could likely increase with the model's ability to represent vertical processes to export carbon to depth.

Active carbon processes that affect TA/DIC in sea ice have contrasting effects on ocean-atmosphere CO₂ fluxes in the Arctic and Antarctic sea-ice zones. In the Arctic, we find a weaker ocean sink for CO₂ which decreases its DIC content. The Antarctic sea-ice zone becomes a weaker source for CO₂ which increases its DIC content. The key difference is the ability of the Southern Ocean to export winter negative alkalinity anomalies, whereas in the Arctic such anomalies remained confined to the surface. The Antarctic carbon pump dominates at a global scale. The simulated numbers are generally small compared to the present-day global ocean annual CO₂ sink (2.6 ± 0.5 Pg C yr⁻¹). However, sea-ice carbon processes seem important at regional (i.e., polar) scales. For instance, sea-ice processes significantly act on the redistribution of DIC and TA within and outside polar basins.

References

- Arrigo KR, Mock T, Lizotte MP. 2010. Primary producers and sea ice, in Thomas DN, Dieckmann GS, eds., *Sea Ice*. 2nd edition. Oxford, UK: Wiley-Blackwell: pp. 282–325.
- Aumont O, Bopp L. 2006. Globalizing results from ocean in situ iron fertilization studies. *Global Biogeochem Cy* 20(2). doi: 10.1029/2005gb002591.
- Aumont O, Ethé C, Tagliabue A, Bopp L, Gehlen M. 2015. PISCES-v2: An ocean biogeochemical model for carbon and ecosystem studies. *Geosci Model Dev* 8(2): 2465–2513. doi: 10.5194/gmd-8-2465-2015.
- Azetsu-Scott K, Starr M, Mei Z-P, Granskog M. 2014. Low calcium carbonate saturation state in an Arctic inland sea having large and varying fluvial inputs: The Hudson Bay system. *J Geophys Res-Oceans* 119(9): 6210–6220. doi: 10.1002/2014JC009948.
- Bopp L, Le Quéré C. 2009. *The Ocean Carbon Cycle* [eBook]. Saltzman E, Quéré CL, eds. 1st edition. Washington, D.C.: Geophysical Monograph Series.
- Brown KA, Miller LA, Mundy CJ, Papakyriakou T, Francois R, et al. 2015. Inorganic carbon system dynamics in landfast Arctic sea ice during the early-melt period. *J Geophys Res-Oceans* 120: 3542–3566. doi: 10.1002/2014JC010620.
- Campin J-M, Marshall J, Ferreira D. 2008. Sea ice-ocean coupling using a rescaled vertical coordinate z^* . *Ocean Model* 24(1–2): 1–14. doi: 10.1016/j.ocemod.2008.05.005.
- Chevallier M, Salas-Mélia D. 2012. The Role of Sea Ice Thickness Distribution in the Arctic Sea Ice Potential Predictability: A Diagnostic Approach with a Coupled GCM. *J Clim* 25(8): 3025–3038. doi: 10.1175/JCLI-D-11-00209.1.
- Clark PU, Dyke AS, Shakun JD, Carlson AE, Clark J, et al. 2009. The Last Glacial Maximum. *Science* 325(5941): 710–714. doi: 10.1126/science.1172873.
- Deal C, Jin M, Elliott S, Hunke E, Maltrud M, et al. 2011. Large-scale modeling of primary production and ice algal biomass within arctic sea ice in 1992. *J Geophys Res-Oceans* 116(C7). doi: 10.1029/2010jc006409.
- Delille B, Jourdain B, Borges AV, Tison J-L, Delille D. 2007. Biogas (CO₂, O₂, dimethylsulfide) dynamics in spring Antarctic fast ice. *Limnol Oceanogr* 52(4): 1367–1379. doi: 10.1029/2004JC002441.

- Delille B, Vancoppenolle M, Geilfus N-X, Tilbrook B, Lannuzel D, et al. 2014. Southern Ocean CO₂ sink: The contribution of the sea ice. *J Geophys Res-Oceans* 119(9): 6340–6355. doi: 10.1002/2014JC009941.
- Dieckmann GS, Nehrke G, Papadimitriou S, Göttlicher J, Steininger R, et al. 2008. Calcium carbonate as ikaite crystals in Antarctic sea ice. *Geophys Res Lett* 35(8). doi: 10.1029/2008gl033540.
- Dieckmann GS, Nehrke G, Uhlig C, Göttlicher J, Gerland S, et al. 2010. Brief communication: Ikaite (CaCO₃*6H₂O) discovered in Arctic sea ice. *The Cryosphere* 4: 227–230.
- Fichefet T, Morales Maqueda MA. 1997. Sensitivity of a global sea ice model to the treatment of ice thermodynamics and dynamics. *J Geophys Res-Oceans* 102(C6): 12609 – 12646.
- Fransson A, Chierici M, Yäger PL, Smith Jr WO. 2011. Antarctic sea ice carbon dioxide system and controls. *J Geophys Res-Oceans* 116(C12). doi: 10.1029/2010jc006844.
- Geilfus N-X, Carnat G, Dieckman GS, Halden N, Nehrke G, et al. 2013. First estimates of the contribution of CaCO₃ precipitation to the release of CO₂ to the atmosphere during young sea ice growth. *J Geophys Res-Oceans* 118(1): 244–255.
- Geilfus N-X, Carnat G, Papakyriakou T, Tison JL, Else B, et al. 2012. Dynamics of pCO₂ and related air-ice CO₂ fluxes in the Arctic coastal zone (Amundsen Gulf, Beaufort Sea). *J Geophys Res-Oceans* 117(C9). doi: 10.1029/2011jc007118.
- Griffies SM, Biastoch A, Böning C, Bryan F, Danabasoglu G, et al. 2009. Coordinated Ocean-ice Reference Experiments (COREs). *Ocean Model* 26(1–2): 1–46. doi: 10.1016/j.ocemod.2008.08.007.
- Large WG, Yeager SG. 2009. The global climatology of an interannually varying air–sea flux data set. *Clim Dynam* 33(2–3): 341–364. doi: 10.1007/s00382-008-0441-3.
- Le Quéré C, Moriarty R, Andrew RM, Canadell JG, Sitch S, et al. 2015. Global Carbon Budget 2015. *Earth Syst Sci Data* 7(2): 349–396. doi: 10.5194/essd-7-349-2015.
- Legge OJ, Bakker DCE, Johnson MT, Meredith MP, Venables HJ, et al. 2015. The seasonal cycle of ocean-atmosphere CO₂ flux in Ryder Bay, west Antarctic Peninsula. *Geophys Res Lett* 42(8): 2934–2942. doi: 10.1002/2015GL063796.
- Ludwig W, Probst J-L, Kempe S. 1996. Predicting the oceanic input of organic carbon by continental erosion. *Global Biogeochem Cy* 10(1): 23–41. doi: 10.1029/95GB02925.
- Miller LA, Papakyriakou TN, Collins RE, Deming JW, Ehn JK, et al. 2011. Carbon dynamics in sea ice: A winter flux time series. *J Geophys Res-Oceans* 116(C2): C02028. doi: 10.1029/2009jc006058.
- Moreau S, Vancoppenolle M, Delille B, Tison J-L, Zhou J, et al. 2015. Drivers of inorganic carbon dynamics in first-year sea ice: A model study. *J Geophys Res-Oceans* 120(1): 471–495.
- Nomura D, Granskog MA, Assmy P, Simizu D, Hashida G. 2013. Arctic and Antarctic sea ice acts as a sink for atmospheric CO₂ during periods of snowmelt and surface flooding. *J Geophys Res-Oceans* 118(12): 6511–6524.
- Notz D, Worster MG. 2008. In situ measurements of the evolution of young sea ice. *J Geophys Res-Oceans* 113(C3). doi: 10.1029/2007jc004333.
- Orr JC, Maier-Reimer E, Mikolajewicz U, Monfray P, Sarmiento JL, et al. 2001. Estimates of anthropogenic carbon uptake from four three-dimensional global ocean models. *Global Biogeochem Cy* 15(1): 43–60.
- Papakyriakou T, Miller L. 2011. Springtime CO₂ exchange over seasonal sea ice in the Canadian Arctic Archipelago. *Ann Glaciol* 52(57): 215–224. doi: 10.3189/172756411795931534.
- Roulet G, Madec G. 2000. Salt conservation, free surface, and varying levels: A new formulation for ocean general circulation models. *J Geophys Res-Oceans* 105(C10): 23927–23942. doi: 10.1029/2000JC900089.
- Rysgaard S, Bendtsen J, Delille B, Dieckmann GS, Glud RN, et al. 2011. Sea ice contribution to the air-sea CO₂ exchange in the Arctic and Southern Oceans. *Tellus B* 63(5): 823–830. doi: 10.1111/j.1600-0889.2011.00571.x.
- Rysgaard S, Bendtsen J, Pedersen LT, Ramløv H, Glud RN. 2009. Increased CO₂ uptake due to sea ice growth and decay in the Nordic Seas. *J Geophys Res-Oceans* 114(C9). doi: 10.1029/2008jc005088.
- Rysgaard S, Glud RN, Lennert K, Cooper M, Halden N, et al. 2012. Ikaite crystals in melting sea ice - Implications for pCO₂ and pH levels in Arctic surface waters. *The Cryosphere* 6(4): 901–908. doi: 10.5194/tc-6-901-2012.
- Rysgaard S, Glud RN, Sejr MK, Bendtsen J, Christensen PB. 2007. Inorganic carbon transport during sea ice growth and decay: A carbon pump in polar seas. *J Geophys Res-Oceans* 112(C3). doi: 10.1029/2006jc003572.
- Rysgaard S, Søgaard DH, Cooper M, Pućko M, Lennert K, et al. 2013. Ikaite crystal distribution in winter sea ice and implications for CO₂ system dynamics. *The Cryosphere* 7: 707–718.
- Saenz BT, Arrigo KR. 2014. Annual primary production in Antarctic sea ice during 2005–2006 from a sea ice state estimate. *J Geophys Res-Oceans* 119(6): 3645–3678. doi: 10.1002/2013JC009677.
- Takahashi T, Sutherland SC, Wanninkhof R, Sweeney C, Feely RA, et al. 2009. Climatological mean and decadal change in surface ocean pCO₂, and net sea-air CO₂ flux over the global oceans. *Deep-Sea Res Pt II* 56(8–10): 554–577.
- Timmermann R, Goosse H, Madec G, Fichefet T, Ethe C, et al. 2005. On the representation of high latitude processes in the ORCA-LIM global coupled sea ice-ocean model. *Ocean Model* 8(1–2): 175–201. doi: 10.1016/j.ocemod.2003.12.009.
- Vancoppenolle M, Fichefet T, Goosse H. 2009. Simulating the mass balance and salinity of Arctic and Antarctic sea ice. 2. Importance of sea ice salinity variations. *Ocean Model* 27(1–2): 54–69. doi: 10.1016/j.ocemod.2008.11.003.
- Vancoppenolle M, Meiners KM, Michel C, Bopp L, Brabant F, et al. 2013. Role of sea ice in global biogeochemical cycles: Emerging views and challenges. *Quaternary Sci Rev* 79: 207–230.
- Wanninkhof R. 1992. Relationship between wind speed and gas exchange over the ocean. *J Geophys Res-Oceans* 97(C5): 7373–7382.
- Zeebe RE, Wolf-Gladrow D. 2001. *CO₂ in Seawater: Equilibrium, Kinetics, Isotopes*. Amsterdam, the Netherlands: Elsevier.

Contributions

- Contributed to conception and design: MV, LB, OA, HG, GM, SM, BD, JLT
- Contributed to the modelling analysis: SM, MV, PYB
- Manuscript writing: SM with comments and inputs from all coauthors

Acknowledgments

We thank very much the Scientific Committee on Ocean Research (SCOR) working group 140 on Biogeochemical Exchange Processes at the Sea Ice Interfaces (BEPsII) for setting the ground for discussions and building projects among the sea-ice biogeochemistry community. We particularly thank Rosina Grimm and Dirk Notz for fruitful discussion of this study. We also thank Jody Deming, Lisa Miller, Leif G. Anderson, and an anonymous reviewer for their very constructive comments that helped to improve the manuscript.

Funding information

We want to thank our funding sources and partners: the F.R.S.-FNRS (FRFC grant no 2.4649.07), the Belgian Science Federal Policy Office (BIGSOUTH project), the European Union (via the projects BISICLO, FP7 CIG 321938) and the MARE project. H.G., B.D. and S.M. are, respectively, senior research associate, research associate and postdoctoral researcher with the F.R.S.-FNRS. S.M. is supported by the Australian Research Council's Special Research Initiative for Antarctic Gateway Partnership (Project ID SR140300001). This is a Mare contribution.

Competing interests

The authors have declared that no competing interests exist.

Data accessibility statement

The model code is available at: <http://www.nemo-ocean.eu/>.

Copyright

© 2016 Moreau et al. This is an open-access article distributed under the terms of the Creative Commons Attribution License, which permits unrestricted use, distribution, and reproduction in any medium, provided the original author and source are credited.